ResearchGate

See discussions, stats, and author profiles for this publication at: https://www.researchgate.net/publication/50832783

Physiologically Based Pharmacokinetic Model of Amphotericin B Disposition in Rats Following Administration of Deoxycholate Formulation (FungizoneA (R)): Pooled Analysis of Publishe...

Article *in* The AAPS Journal · March 2011

DOI: 10.1208/s12248-011-9267-8 · Source: PubMed

CITATIONS
21

READS
399

4 authors, including:

Pavel Gershkovich
University of Nottingham
106 PUBLICATIONS **1,912** CITATIONS

SEE PROFILE

Kishor M Wasan
University of Saskatchewan
310 PUBLICATIONS **9,263** CITATIONS

SEE PROFILE

Donald E Mager
University at Buffalo, The State University of New York
234 PUBLICATIONS **6,406** CITATIONS

SEE PROFILE

Some of the authors of this publication are also working on these related projects:

Eritoran (E5564) Research View project

Organophosphate toxicity View project

All content following this page was uploaded by Kishor M Wasan on 19 May 2014.

The user has requested enhancement of the downloaded file.

The AAPS Journal, Vol. 13, No. 2, June 2011 (© 2011)
DOI: 10.1208/s12248-011-9267-8

Research Article

Physiologically Based Pharmacokinetic Model of Amphotericin B Disposition in Rats Following Administration of Deoxycholate Formulation (Fungizone®): Pooled Analysis of Published Data

Leonid Kagan,[1,3] Pavel Gershkovich,[2] Kishor M. Wasan,[2] and Donald E. Mager[1]

Received 17 January 2011; accepted 25 February 2011; published online 23 March 2011

Abstract. The time course of tissue distribution of amphotericin B (AmB) has not been sufficiently characterized despite its therapeutic importance and an apparent disconnect between plasma pharmacokinetics and clinical outcomes. The goals of this work were to develop and evaluate a physiologically based pharmacokinetic (PBPK) model to characterize the disposition properties of AmB administered as deoxycholate formulation in healthy rats and to examine the utility of the PBPK model for interspecies scaling of AmB pharmacokinetics. AmB plasma and tissue concentration–time data, following single and multiple intravenous administration of Fungizone® to rats, from several publications were combined for construction of the model. Physiological parameters were fixed to literature values. Various structural models for single organs were evaluated, and the whole-body PBPK model included liver, spleen, kidney, lung, heart, gastrointestinal tract, plasma, and remainder compartments. The final model resulted in a good simultaneous description of both single and multiple dose data sets. Incorporation of three subcompartments for spleen and kidney tissues was required for capturing a prolonged half-life in these organs. The predictive performance of the final PBPK model was assessed by evaluating its utility in predicting pharmacokinetics of AmB in mice and humans. Clearance and permeability–surface area terms were scaled with body weight. The model demonstrated good predictions of plasma AmB concentration–time profiles for both species. This modeling framework represents an important basis that may be further utilized for characterization of formulation- and disease-related factors in AmB pharmacokinetics and pharmacodynamics.

KEY WORDS: amphotericin B; interspecies scaling; physiologically based pharmacokinetic model; tissue distribution.

INTRODUCTION

Amphotericin B (AmB) is a polyene antibiotic that was discovered more than 50 years ago for treatment of systemic fungal and parasitic infections. An important clinical advantage of AmB is that only a few cases of resistance to this drug have been reported (1). Nephrotoxicity is a major side effect of AmB that usually requires discontinuation of the treatment. Several acute adverse reactions (fever, chilling, and rigor) might also necessitate slowing of the infusion rate. A deoxycholate micellar dispersion (Fungizone®) was the first available intravenous (IV) formulation of AmB. Other particulate formulations have been developed (*e.g.*, liposomal AmBisome® and lipid complex Abelect®), which demonstrate similar efficacy and lower toxicity profiles. All currently available commercial formulations used in the clinic must be administered parenterally. The lack of an affordable oral delivery system, as well as high costs of the existing treatments, significantly limits AmB availability for patients especially in developing countries.

The amphiphilic nature of AmB results in a very low solubility, both in water (at physiological pH) and organic solvents (1). In addition, it has very low membrane permeability and falls into class IV of the Biopharmaceutical Classification System (2). Conventional formulations of AmB exhibit very low oral bioavailability; however, several promising reports have emerged for novel AmB oral delivery systems (3–5).

Despite its extensive clinical use, the relationship between the pharmacokinetics and the pharmacodynamics of AmB is not completely understood. In fact, no correlation between plasma AmB concentrations and drug response has been established (6,7). A variety of complexities in AmB disposition might complicate data analysis. The drug significantly binds to albumin, α1-acid glycoprotein and lipoproteins, with unusual nonlinear binding behavior reported in humans (8). No metabolic pathway has been identified for AmB (9), and biliary and metabolic clearances only account for 3–40% of total elimination, which is species dependent (10). AmB shows significant tissue distribution and prolonged

[1] Department of Pharmaceutical Sciences, University at Buffalo, The State University of New York, 363 Hochstetter Hall, Buffalo, New York 14260, USA.
[2] Faculty of Pharmaceutical Sciences, The University of British Columbia, Vancouver, British Columbia V6T 1Z3, Canada.
[3] To whom correspondence should be addressed. (e-mail: lkagan@buffalo.edu)

 1550-7416/11/0200-0255/0 © 2011 American Association of Pharmaceutical Scientists

tissue storage as evidenced by a high volume of distribution, slow rates of transfer from a peripheral compartment in comparison to rate of transfer to the peripheral compartment, as well as high tissue concentrations relative to plasma (11). The distribution of AmB is highly dependent on pharmaceutical formulation (3,12,13), and disease status may also influence the degree of accumulation of AmB in tissues (14).

The interest in developing physiologically based pharmacokinetic (PBPK) models is growing as they provide a more mechanistic approach for studying drug disposition and predicting human pharmacokinetics from preclinical research (15). This type of model may also allow for incorporating disease-related changes in physiology and assessment of their effects on drug distribution. We hypothesize that the development of a PBPK model can improve understanding of AmB pharmacokinetics and pharmacodynamics, may be utilized for evaluating therapy with existing AmB formulations, and guide development of novel formulations and routes of administration.

To our knowledge, no mathematical model of AmB kinetics in tissues has been reported. The goal of this work was to develop and evaluate a PBPK model to characterize the disposition properties of AmB administered as deoxycholate formulation in healthy rats. The second goal was to examine the utility of the PBPK model for interspecies scaling of AmB pharmacokinetics. For more complex formulations of AmB (*e.g.*, AmBisome®), the overall disposition and elimination is governed by a combination of properties of the released and formulation-associated drug. It is hypothesized that following Fungizone® administration, the concentration of the formulation falls rapidly below a critical micellar concentration, and AmB disposition is mainly driven by the properties of the drug molecule itself (*i.e.*, there is no significant effect of the formulation on pharmacokinetics). Therefore, it is essential to initially develop a model of AmB pharmacokinetics following Fungizone® administration.

METHODS

Data Sources

Three studies were identified that report both plasma and tissue pharmacokinetic data of AmB following single IV administration in rats. These studies mainly focused on AmB disposition into target tissues (liver, kidney, and spleen) and contained very limited data on other tissues. Gershkovich and colleagues reported plasma pharmacokinetic profiles and tissue concentrations (liver, kidney, spleen, lung, and heart) at 72 h following IV injection of AmB (Fungizone®, 0.8 mg/kg) to male Sprague–Dawley rats (3). Fielding and colleagues reported plasma profiles and tissue concentrations at 0.5 and 24 h (for liver, kidney, and spleen, 4 and 96 h were also available) following IV injection of AmB (Fungizone®, 1 mg/kg) to male Crl:CD(SD)BR rats (13). Angra and colleagues reported plasma pharmacokinetic profiles and tissue concentrations at 120 h following IV injection of AmB (Amfocan®, another deoxycholate formulation, 2 mg/kg) to male Sprague–Dawley rats (16). Mean data in each publication were captured by computer digitization and combined to create a common single dose dataset which was used for development of the PBPK model. A single study by Wang and co-workers contained pharmacokinetic data following multiple IV doses (1 mg/kg daily for 14 days) of AmB (Fungizone®) administered to male Crl:CD(SD)BR rats (17). Tissue concentrations 24 h after the last dose and tissue half-lives were reported. This information was used to calculate concentrations in tissues on Days 5 and 14 after the last dose (thereby simulating sampling times of the original study). It was assumed that there is no difference in AmB disposition between different rat strains and mean rat body weight was assumed to be 250 gr. Drug concentrations were normalized to a 1-mg/kg dose level, as systemic clearance and volume of distribution are dose independent (18,19). Plasma concentration–time profiles of AmB following administration of deoxycholate formulation as an IV bolus injection of 1 mg/kg to mice (20) and a 2-h IV infusion of 0.6 mg/kg to humans (12) were used to evaluate interspecies scaling of the final PBPK model.

Physiological Parameters

Physiological parameters, such as tissue weights, fractions of vascular space in tissues, and plasma flow rates to different organs, were fixed to literature values reported in Table I (21–23). Plasma cardiac output (CO) for rats and mice were calculated using an allometric relationship, as follows: $CO_{rat}(L/h) = 14.1 \cdot (1-\text{Hematocrit}) \cdot (\text{body weight in kilograms})^{0.75}$ and $CO_{mouse}\ (L/h) = 16.5 \cdot (1-\text{Hematocrit}) \cdot (\text{body weight in kilograms})^{0.75}$; and blood cardiac output for humans (70 kg) was fixed to 312 L/h (21). All tissues that were not sampled were lumped into a remainder compartment (24). Fraction unbound in plasma (f_u^{pl}) for mice, rats, and humans were fixed to 0.074, 0.11, and 0.052 (20). A density of 1 was assumed for all tissues.

AmB Elimination Mechanisms

A wide range of total clearance values of AmB are reported in rats, and some of the variability can be related to the experimental methods, such as lower limit of quantification of the analytical assay and duration of sampling. In humans, the unbound renal clearance is similar to glomerular filtration rate (GFR) (8). Accordingly, the renal clearance of AmB was calculated using $f_u^{pl} \cdot GFR$. GFR was calculated using an allometric relationship, as follows: $GFR(L/h) = 0.3 \cdot (\text{body weight in kilograms})^{0.75}$ (25). This method provided a value of AmB renal clearance that is similar to literature values (19). The biliary clearance of AmB was fixed to 20% of total systemic clearance (17). As renal and biliary clearances account for less than 50% of elimination, incorporation of an additional elimination pathway was required for capturing the data, which was assigned to the remainder compartment (CL_{rm}).

PBPK Model Development and Modeling Strategy

Analysis of the data and construction of the PBPK were performed in several stages. For initial assessment of AmB pharmacokinetics, a non-compartmental analysis of the data was conducted. The half-lives and partition coefficients (defined as the tissue–plasma ratio of area under the

Table I. Physiological Parameters for Mouse, Rat, and Human

	Plasma flow, % of cardiac output			Tissue volume, % of body weight			Fraction of the vascular space, %		
Tissue	Mouse	Rat	Human	Mouse	Rat	Human	Mouse	Rat	Human
Liver	16.1	18.3	22.7	5.49	3.66	2.57	31	21	11
Kidneys	9.1	14.1	17.5	1.67	0.73	0.44	24	16	36
Spleen	1.125[c]	1.0 [c]	1.38[c]	0.35	0.2	0.26	17	22	22[e]
GI tract	12.87[d]	14.3[c]	16.7[d]	4.22	2.7	1.71	–[a]	–[a]	–[a]
Heart	6.6	4.9	4.0	0.5	0.33	0.47	–[a]	–[a]	–[a]
Lungs	100	100	100	0.73	0.5	0.76	50	36	36[e]
Muscle	–[a]	–[a]	–[a]	–[a]	–[a]	–[a]	4[b]	4[b]	1[b]

Data extracted from (21), except as noted
[a] Not used in the model
[b] Value used for the remainder compartment
[c] Mean value from (22) and (23)
[d] Calculated as portal hepatic flow–spleen flow
[e] Human data unavailable, the value for rat was used in the model

concentration curves) were calculated using the linear trapezoidal rule.

At stage 1, the AmB plasma concentration–time profile was described by an explicit bi-exponential equation and different structural models for organs were evaluated independently (Fig. 1). In model A, the organ was represented as a single "well-stirred" compartment (where the venous plasma is considered to be in instant equilibrium with the tissue concentration) and characterized by a partition coefficient $\left(K_p^{tissue} = f_u^{pl}/f_u^{tissue}\right)$. In model B, the organ was divided into two subcompartments (vascular and extravascular) with a permeability-limited distribution (PS_{tissue}) and tissue-specific unbound fraction (f_u^{tissue}). Model C, in addition to vascular and extravascular spaces, included an additional "deep tissue" subcompartment that was characterized by first-order association (k_a) and dissociation (k_d) rate constants. Model selection was performed using a visual inspection of the model-fitted profiles.

At stage 2, a whole-body PBPK model was constructed (Fig. 2). Additional organs were added to the model (lungs, gut, and heart), and since only a limited number of observations were available for these tissues, they were assumed to have a "well-stirred" structure (model A). The remainder compartment encompassed all nonsampled tissues. The following equations were used to describe the model structure for AmB disposition following single IV administration:

Plasma (pl):

$$V_{pl}\frac{dC_{pl}}{dt} = Q_{co}\left(\frac{C_{lu}}{Kp_{lu}} - C_{pl}\right) \quad (1)$$

Gastrointestinal tract (gi) and heart (ht):

$$V_{ti}\frac{dC_{ti}}{dt} = Q_{ti}\left(C_{pl} - \frac{C_{ti}}{Kp_{ti}}\right) \quad (2)$$

Spleen (sp):

$$V_{sp,vas}\frac{dC_{sp,vas}}{dt} = Q_{sp}\left(C_{pl} - C_{sp,vas}\right) - PS_{sp}\left(f_u^{pl}C_{sp,vas} - f_u^{sp}C_{sp,exv}\right) \quad (3)$$

$$V_{sp,exv}\frac{dC_{sp,exv}}{dt} = PS_{sp}\left(f_u^{pl}C_{sp,vas} - f_u^{sp}C_{sp,exv}\right) - Ka_{sp}f_u^{sp}C_{sp,exv}V_{sp,exv} + Kd_{sp}A_{sp,deep} \quad (4)$$

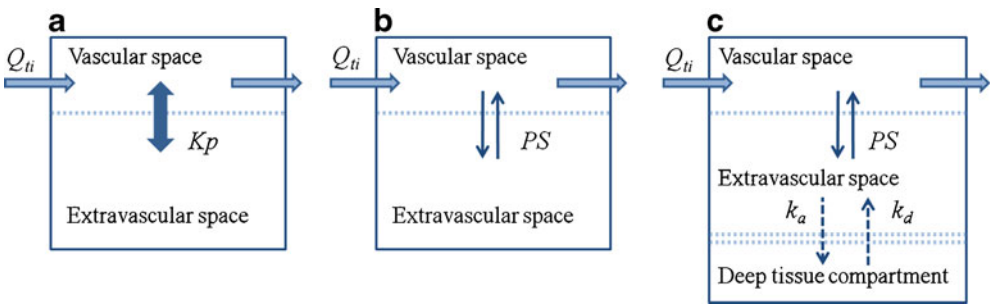

Fig. 1. Model structures evaluated for major target organs (liver, kidney, and spleen). **a** Model A, single "well-stirred" compartment where the venous plasma concentration is in instant equilibrium with the tissue concentration governed by a partition coefficient (*Kp*). **b** Model B, two subcompartments (vascular and extravascular) with a permeability-limited distribution (*PS*). **c** Model C, three subcompartments (vascular, extravascular, and deep tissue) characterized by permeability-limited distribution and rates of association with (k_a) and dissociation from (k_d) deep tissue subcompartment. Q_{ti}, plasma flow rate to the organ

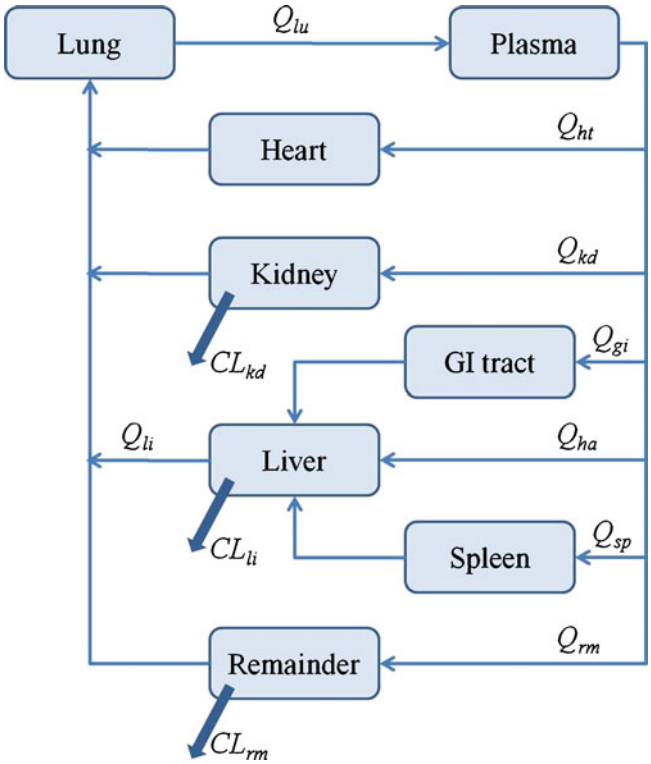

Fig. 2. Schematic of the whole-body PBPK model used to characterize the biodistribution of AmB in rats, mice, and humans. Q_{ti}, plasma flow rate to the organ; Cl_{ti}, organ clearance

$$\frac{dA_{sp,deep}}{dt} = Ka_{sp} f_u^{sp} C_{sp,exv} V_{sp,exv} - Kd_{sp} A_{sp,deep} \quad (5)$$

Liver (li):

$$V_{li}\frac{dC_{li}}{dt} = Q_{ha}C_{pl} + Q_{sp}\frac{C_{sp}}{Kp_{sp}} + Q_{gi}\frac{C_{gi}}{Kp_{gi}} - Q_{li}\frac{C_{li}}{Kp_{li}} - Cl_{li} f_u^{pl}\frac{C_{li}}{Kp_{li}} \quad (6)$$

Kidney (kd):

$$V_{kd,vas}\frac{dC_{kd,vas}}{dt} = Q_{kd}\left(C_{pl} - C_{kd,vas}\right) - PS_{kd}\left(f_u^{pl}C_{kd,vas} - f_u^{kd}C_{kd,exv}\right) - Cl_{kd} f_u^{pl} C_{kd,vas} \quad (7)$$

$$V_{kd,exv}\frac{dC_{kd,exv}}{dt} = PS_{kd}\left(f_u^{pl}C_{kd,vas} - f_u^{kd}C_{kd,exv}\right) \quad (8)$$

Lung (lu):

$$V_{lu}\frac{dC_{lu}}{dt} = Q_{li}\frac{C_{li}}{Kp_{li}} + Q_{ht}\frac{C_{ht}}{Kp_{ht}} + Q_{kd}C_{kd,vas} + Q_{rm}C_{rm,vas} - Q_{co}\frac{C_{lu}}{Kp_{lu}} \quad (9)$$

Remainder (rm):

$$V_{rm,vas}\frac{dC_{rm,vas}}{dt} = Q_{rm}\left(C_{pl} - C_{rm,vas}\right) - PS_{rm}\left(f_u^{pl}C_{rm,vas} - f_u^{rm}C_{rm,exv}\right) \quad (10)$$

$$V_{rm,exv}\frac{dC_{rm,exv}}{dt} = PS_{rm}\left(f_u^{pl}C_{rm,vas} - f_u^{rm}C_{rm,exv}\right) - Cl_{rm} f_u^{rm} C_{rm,exv} \quad (11)$$

where Q_{ti} is tissue plasma flow, and V_{ti} is tissue volume ($V_{ti,vas}$ and $V_{ti,exv}$ are the volumes of the vascular and extravascular subcompartments). The initial conditions for Eqs. 1, 2, 3, 4, 5, 6, 7, 8, 9, 10, 11 were all set to zero.

At stage 3, all parameters estimated during stages 1 and 2 were kept constant, and the predictive power of the PBPK model was assessed using the AmB multiple dose data set (17). Separate data for the muscle tissue were not available in any of the single dose studies; hence, muscle was included in the remainder compartment during model development. In the multiple dose study, the concentrations for muscle tissue had been measured and were compared against concentrations in the remainder compartment predicted by the model.

At stage 4, the proposed PBPK model was fitted simultaneously to both single dose and multiple dose data. All parameters were shared between single and multiple dose data sets. In addition, to further improve the model, the structure was modified to incorporate a "deep tissue" subcompartment for kidney tissue (Eq. 8 was substituted by Eqs. 12 and 13):

$$V_{kd,exv}\frac{dC_{kd,exv}}{dt} = PS_{kd}\left(f_u^{pl}C_{kd,vas} - f_u^{kd}C_{kd,exv}\right) - Ka_{kd} f_u^{kd} C_{kd,exv} V_{kd,exv} + Kd_{kd} A_{kd,deep} \quad (12)$$

$$\frac{dA_{kd,deep}}{dt} = Ka_{kd} f_u^{kd} C_{kd,exv} V_{kd,exv} - Kd_{kd} A_{kd,deep} \quad (13)$$

At stage 5, plasma profiles of AmB following IV administration to mice and humans were simulated using the final PBPK model. Body weights of 24 gr and 70 kg were assumed, and rat physiological parameters (organ volumes, blood flows, and fraction of vascular space in the tissues) were replaced with corresponding values for mouse or human (Table I). Species-specific f_u^{pl} values were used, whereas Kp_{ti}, f_u^{ti}, ka_{ti}, and kd_{ti} were assumed to be identical among the species. Cl_{ti} and PS_{ti} were predicted from the values estimated for rats using an allometric equation:

$$P = P_{rat}\left(\frac{BW}{BW_{rat}}\right)^{B} \quad (14)$$

where P is the parameter of interest, BW is species body weight, and B is an allometric exponent (fixed to 0.75 for renal and biliary clearances). For Cl_{rm} the value of B was fixed to 1. It was assumed that permeability of tissues for

AmB is similar and that surface area is proportional to $BW^{0.67}$. Thus, the value of B was fixed to 0.67 for PS_{ti} (26).

Data Analysis

The ADAPT 5 program (Biomedical Simulations Resource, USC, Los Angeles, CA) was used for single-organ modeling, and the whole-body PBPK was constructed using MATLAB R2008a (The MathWorks, Natick, MA). All parameters were estimated using maximum likelihood, and the variance model was defined as:

$$\mathrm{VAR}_i = (\sigma_1 + \sigma_2 \cdot Y(\theta, t_i))^2 \quad (15)$$

where VAR_i is the variance of the ith data point, σ_1 and σ_2 are the variance model parameters, and $Y(\theta, t_i)$ is the ith predicted value from the pharmacokinetic model. The goodness-of-fit was assessed by system convergence, Akaike Information Criterion, estimator criterion value for the maximum likelihood method, examination of residuals, and visual inspection.

RESULTS

Non-compartmental Analysis

Overall pharmacokinetic parameters of AmB for three plasma concentration–time profiles following the administration of a single IV dose (3,13,16) and for the combined data set are summarized in Table II. Tissue half-lives of AmB following administration of single IV dose (calculated for the common data set) were 22, 35, 41, and 31 h for liver, kidney, spleen, and lungs, respectively. AmB significantly distributed into tissue, and partition coefficients were 35, 25, 89, and 75 for liver, kidney, spleen, and lungs. The direct calculation of parameters for other tissues was not possible due to insufficient data.

Stage 1: Single-Organ Models

Three competing model structures (Fig. 1) were evaluated for the liver, kidney, and spleen using a fixed explicit bi-exponential driving function for plasma concentrations. The simplest model structure that was able to describe the shape of the concentration–time profile in the tissue was selected. The liver profile could be modeled using a single parameter (partition coefficient, model A). A longer AmB half-life in kidneys necessitated inclusion of a permeability-limited distribution (model B). The most complex concentration–time profile was observed in the spleen, which was characterized by a rapid increase in concentrations and a prolonged terminal phase. Incorporation of a "deep tissue" subcompartment (model C) was required to satisfactorily capture the shape of the AmB pharmacokinetic profile in this organ (Fig. 3).

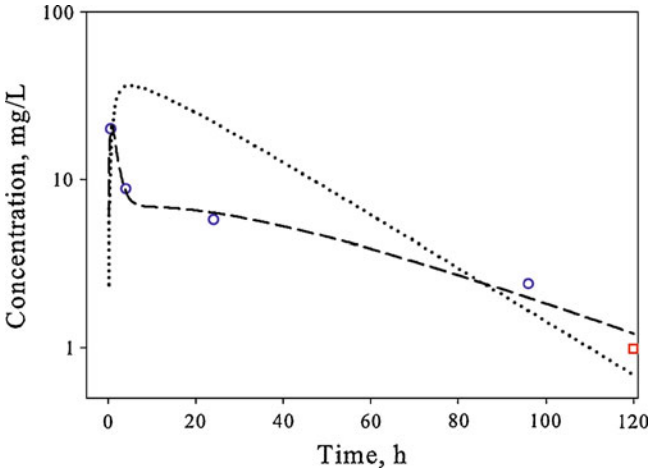

Fig. 3. Time course of AmB in the spleen of rats following single IV bolus administration. The symbols represent data extracted from references (*white circle*, (13) and *white square*, (16)), and *lines* are model-predicted profiles after fitting single-organ spleen data to model B (*dotted line*) and model C (*dashed line*)

Stage 2: Whole Body PBPK Model for Single IV Dose

A whole-body PBPK model was constructed according to the scheme presented in Fig. 2 using organ structures defined during stage 1. Additional organs (lungs, gut, and heart) with limited number of observations were included and assumed to have a "well-stirred" structure (model A). The proposed PBPK model allowed for a good simultaneous description of the experimental data from several studies in plasma (Fig. 4) and tissues (Fig. 5), and estimated pharmacokinetic parameters are shown in Table III. Due to sparse sampling, parameters describing the spleen compartment could not be estimated with sufficient precision using the whole-body model, and were fixed to values estimated during stage 1.

In order to estimate intrinsic clearance parameters from the liver and kidney compartments, cumulative urinary and biliary excretion profiles were constructed using the plasma concentration–time profile described by an explicit function. Renal and biliary AmB clearances were calculated as described in the method section. Intrinsic organ clearances

Table II. Global AmB Pharmacokinetic Parameters in Rats Obtained by Non-Compartmental Analysis

		Data set			
Parameter	Units	Gershkovich *et al.*, 2009 (3)	Angra *et al.*, 2009 (16)	Fielding *et al.*, 1991 (13)	Combined
AUC	mg · h/L	6.29	6.75	7.00	6.63
CL	L/(h · kg)	0.16	0.15	0.14	0.15
V_{ss}	L/kg	2.90	3.16	3.78	3.63
$T_{1/2}$	h	14.5	21.9	15.2	18.0

AUC area under the plasma concentration–time curve, *CL* clearance, V_{ss} steady-state volume of distribution, $T_{1/2}$ terminal half-life

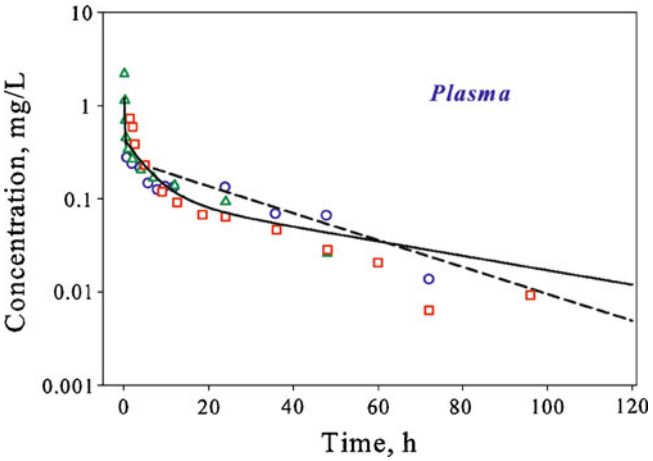

Fig. 4. Time course of plasma AmB in rats following single IV bolus administration. Symbols represent data extracted from references (*white circle*, (13); *white square*, (16); and *triangles*, (3)), and *lines* are whole-body PBPK model predicted profiles after fitting to single dose data (*dashed line*) and simultaneous fitting to the single and multiple dose data (*solid line*)

were estimated using these excretion profiles during initial model runs and were fixed during the final model run. As renal and biliary excretion processes were shown to account for less than 50% of total AmB elimination, an additional clearance mechanism was required for capturing the data (0.110 L/h). In addition, incorporation of permeability-limited distribution into the structure of the remainder compartment was required.

Stage 3: Simulations of Multiple IV Dose Administration

To evaluate the performance of the proposed PBPK model, a simulation for multiple dosing was performed using the model structure and parameters determined at previous stages. Model predictions were compared with experimental data obtained following IV administration of AmB (Fungizone®) to rats for 14 days (17). Reasonable predictions of tissue concentrations were obtained for liver, spleen, lung, and heart (Fig. 6, dashed line). Concentrations in muscle were unavailable in single dose studies, and muscle tissue was incorporated into the remainder compartment of the model. Muscle constituted approximately 50% of the mass of the remainder compartment. The model reasonably captured muscle concentrations following multiple dose administration using equations for the remainder compartment. However, concentrations in the kidney compartment were significant underestimated, and the observed half-life of AmB in the kidney was much longer than predicted.

Stage 4: Simultaneous Fit of Single and Multiple Dose Data

To improve model performance and the precision of estimated parameters, a simultaneous fit was performed using both single and multiple dose data. The initial model structure was unable to capture the data from the kidney compartment (data not shown). Thus, the model for the kidney compartment was modified to include a "deep tissue" subcompartment (Fig. 1, model C). The final model resulted in a good simultaneous description of both single and multiple dose data sets (Figs. 4, 5, and 6) and allowed for the estimation of all model parameters with sufficient precision (Table III).

Stage 5: Interspecies Scaling

To validate the final PBPK model, the ability of the model to predict AmB pharmacokinetics in other species was evaluated. AmB plasma concentration–time profiles in mice

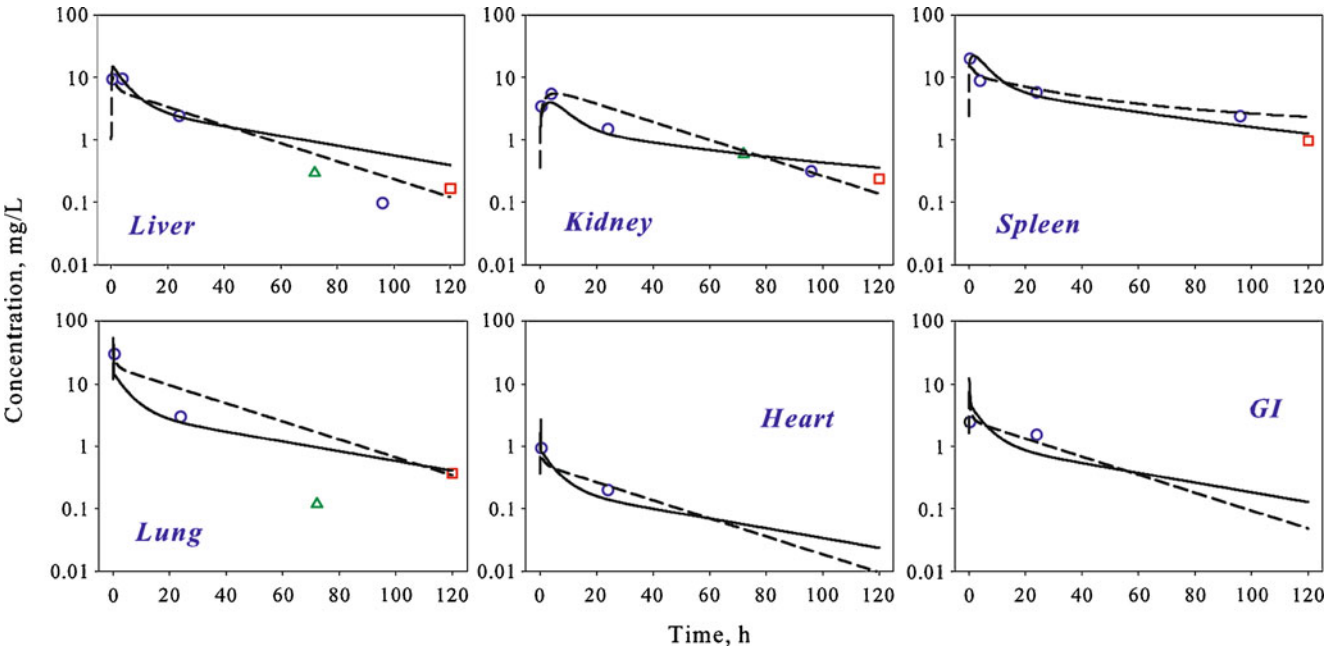

Fig. 5. Time course of AmB in different tissues of rats following single IV bolus administration. Symbols represent data extracted from references (*white circle*, (13); *white square*, (16); and *triangle*, (3)), and *lines* are whole-body PBPK model predicted profiles after fitting to single dose data (*dashed line*) and simultaneous fitting to the single and multiple dose data (*solid line*)

Table III. Estimated Pharmacokinetic Parameters of AmB in Rats Using a PBPK Model

Parameter	Units	Single dose only (stage 2)		Single and multiple dose (stage 4)	
		Estimate	% CV	Estimate	% CV
Kp_{gi}		9.75	17	10.7	18
Kp_{lu}		70.1	15	34.3	15
Kp_{ht}		2.0	19	2.0	14
Kp_{li}		24.4	13	33.0	11
Cl_{li}	L/h	6.00×10^{-2}	–[a]	6.00×10^{-2}	–[a]
f_u^{kd}		4.30×10^{-3}	14	7.26×10^{-3}	19
PS_{kd}	L/h	1.15×10^{-1}	28	7.50×10^{-2}	31
Ka_{kd}	h^{-1}	–[b]	–	2.58×10^{-1}	34
Kd_{kd}	h^{-1}	–[b]	–	1.29×10^{-3}	66
Cl_{kd}		1.00×10^{-1}	–[a]	1.00×10^{-1}	–[a]
f_u^{sp}		2.70×10^{-3}	–[c]	1.71×10^{-3}	17
PS_{sp}	L/h	7.47	–[c]	5.98×10^{-1}	26
Ka_{sp}	h^{-1}	9.32	–[c]	9.05×10^{-1}	33
Kd_{sp}	h^{-1}	2.37×10^{-2}	–[c]	4.56×10^{-3}	20
f_u^{rm}		5.00×10^{-2}	16	1.60×10^{-2}	11
PS_{rm}	L/h	2.12	33	5.47×10^{-1}	16
Cl_{rm}	L/h	1.10×10^{-1}	17	1.58×10^{-1}	15

[a] Fixed to match previously reported values
[b] Not estimated
[c] Fixed to estimate from single-organ model

and humans were simulated by scaling parameters estimated for rats. The model predicted profiles are in good agreement with experimental data (Fig. 7).

DISCUSSION

AmB remains a drug of choice for many serious fungal infections, despite toxicities associated with treatment and development of newer therapeutic alternatives. In addition, AmB is an important agent in treatment of several parasitic protozoan infections, including leishmaniasis, Chaga's disease, and primary amoebic meningoencephalitis. Leishmaniasis infection is considered one of the "most neglected diseases" (27) and ranked second in mortality among tropical diseases (28). Although lipid-based formulations that are less toxic currently prevail in clinical use, it was essential to investigate the behavior of the deoxycholate dispersion. This enabled characterization of AmB distribution properties without the interplay of complex particulate formulations. In addition, the deoxycholate formulation is frequently used as a

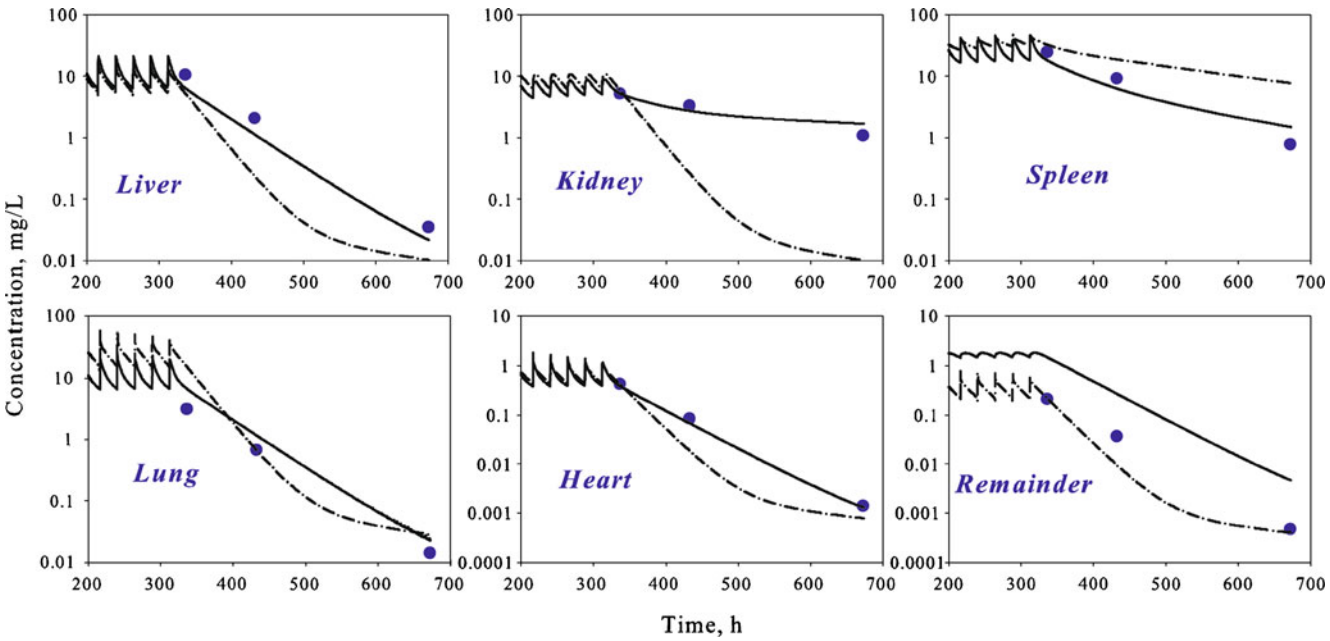

Fig. 6. Time course of AmB in different tissues of rats following multiple IV bolus administration. Symbols represent data extracted from reference (*black circle*, (17)), and *lines* are whole-body PBPK model predicted profiles after simulation using parameters estimated from single dose data (*dashed–dotted line*) and simultaneous fitting to the single and multiple dose data (*solid line*). For the remainder compartment, symbols represent concentration in muscle tissue

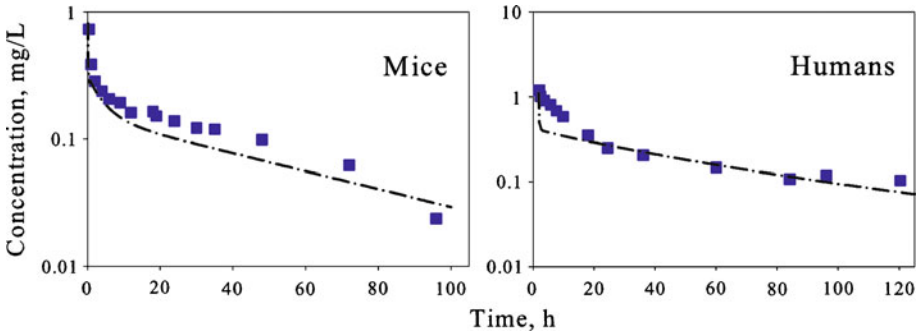

Fig. 7. Time course of plasma AmB concentrations in mice and humans following single IV bolus administration. Symbols represent data extracted from references (*black square*, (20) and *black square*, (12)), and *lines* are whole-body PBPK model predicted profiles after simulation using interspecies scaling of parameters estimated using rat data

control in preclinical disposition and activity studies for newly developed AmB delivery systems.

The physicochemical properties of AmB dictate its extensive distribution and prolonged retention in various tissues. No correlation between plasma AmB pharmacokinetics and clinical outcomes has been established (6,7). One hypothesis is that the therapeutic effect of AmB is related to its concentrations inside target organs. Development of a model for predicting the time course of drug concentrations inside target tissues may improve understanding of concentration–activity relationships for AmB. In this work, the PBPK model of AmB following administration of the deoxycholate formulation was developed and provided a good simultaneous description of experimental plasma and tissue AmB pharmacokinetic data in rats (Figs. 4, 5, and 6). Furthermore, a successful prediction of plasma concentration–time profiles in mice and humans was obtained by scaling parameters estimated for rat species (Fig. 7).

Several AmB pharmacokinetic–pharmacodynamic studies have been performed in rats and most focused on tissue distribution. However, none of the individual studies contain sufficient data for characterizing the full time course of AmB in organs or for constructing of a PBPK model. Combining information from several publications was essential for identifying the structural framework of organs and for estimating parameters with sufficient precision. The dose-normalized plasma concentration–time profiles from these studies were very similar (Fig. 4), which can be used as a partial validation for this approach. Due to the slow nature of distribution processes, inclusion of both single and multiple dose data was critical for resolving the structural model for the kidney compartment. The available data set contained limited information on the initial tissue distribution, which can influence parameter identifiability, and this should be investigated in future studies.

A major component of total AmB clearance has yet to be characterized. The drug undergoes urinary and biliary excretion; however, these pathways account for less than 50% of elimination (10), and no metabolites have been identified (9,29). To capture the data, an additional elimination pathway had to be incorporated into the PBPK model. For simplicity, this clearance was assigned to the remainder compartment; however, the nature of this process remains unknown. One possibility is that it represents binding of AmB to cell membranes inside tissues. The drug is then released back to the plasma at a very slow rate, such that plasma concentrations remain under the limit of detection for existing analytical methods. Under such conditions, tissue binding might actually manifest as an apparent clearance. Tissue data utilized in the model were based on concentrations in homogenized samples. No information is currently available on AmB concentrations in different tissue subcompartments (*e.g.*, interstitial fluid and cell fraction), which could be important for treatment of intra- and extracellular infections. The developed PBPK model mainly focuses on target organs for AmB therapy of fungal infections and visceral leishmaniasis. Further research is needed to include other tissues, such as muscle (target organ in treatment of Chagas disease), skin (target organ in cutaneous leishmaniasis), bone, and fat, which constitute up to 70% of body mass.

The biodistribution of lipid-based AmB formulations (*e.g.*, liposomal AmBisome® and lipid complex Abelect®) is different from the distribution of AmB administered as deoxycholate dispersion. These differences arise from recognition and uptake of particulates by macrophage cells of the reticuloendothelial system, which results in greater concentrations in liver and spleen as compared to Fungizone®. Plasma pharmacokinetics can also vary among different lipid-based systems, and this is attributed to the effect of the size of particulates on the uptake rate by phagocytic cells (3). The pharmacokinetics of AmB following administration of lipid-based formulations is probably governed by a combination of properties of formulation-associated AmB and drug released from the formulation. In addition, disease states can affect the disposition of AmB. Concentration of AmB in liver and spleen of leishmaniasis-infected mice were significantly lower than in non-infected animals following administration of AmBisome®. Differences were also correlated with the rate of disease progression in different organs (14). These effects might be attributed to impairment in the function of the reticuloendothelial system caused by infection. In fact, it has been demonstrated *in vitro* that the phagocytic activity of macrophages infected by *Leishamnia donovani* is less efficient than that of non-infected cells (30). Our PBPK model for AmB represents a platform that can be further modified to encompass both formulation- and disease-related effects on AmB disposition and elimination in the future.

One of the purposes of pharmacokinetic modeling is to understand interspecies differences and to predict drug

behavior in humans from preclinical data. Several attempts of scaling plasma AmB PK were reported, where allometric coefficients and exponents were obtained empirically by plotting corresponding parameters (*e.g.*, clearance, volume, mean residence time, and half-life) against species body weights (10,20). The predictive performance of our final PBPK model was assessed by evaluating its utility in predicting PK of AmB in mice and humans. The model demonstrated good predictions of plasma AmB concentration–time profiles for both species (Fig. 7). The scaling was done by combining species-specific physiological parameters and model parameters that were scaled with body weight using theoretically expected allometric exponents (31). One advantage of the physiologically based approach is an inherent ability to describe the time course of drugs in various tissues. Combining PBPK modeling with allometry can provide a mechanism for predicting AmB concentrations in human organs that cannot be readily assessed experimentally.

Various animal models of human disease are often utilized in preclinical drug development. Specifically, AmB activity has been evaluated in mice (14), rats (32), hamsters (33), and dogs (34). Unfortunately, pharmacodynamic studies are rarely accompanied by a thorough biodistribution investigation in the same species. The PBPK modeling approach allows for sharing of a common model structure and known parameters. Thus, data from separate studies can be analyzed simultaneously and missing data from one trial can be complemented by information from another trial.

CONCLUSION

In the current study, a PBPK model for AmB administered as a deoxycholate formulation was developed using rat data and validated by predicting pharmacokinetic profiles in other species. The model successfully described various factors influencing AmB pharmacokinetics and helped identify future experimentation required for resolving complexities in its biodistribution. This modeling framework represents an important basis that can be further utilized for characterization of formulation- and disease-related factors in AmB pharmacokinetics and pharmacodynamics and for understanding the extent and time course of absorption from newly developed oral formulations.

ACKNOWLEDGMENTS

The authors would like to thank Dr. John M. Harrold for his help in developing a MATLAB code for this project.

REFERENCES

1. Lemke A, Kiderlen AF, Kayser O. Amphotericin B. Appl Microbiol Biotechnol. 2005;68(2):151–62.
2. Amidon GL, Lennernas H, Shah VP, Crison JR. A theoretical basis for a biopharmaceutic drug classification: the correlation of *in vitro* drug product dissolution and *in vivo* bioavailability. Pharm Res. 1995;12(3):413–20.
3. Gershkovich P, Wasan EK, Lin M, Sivak O, Leon CG, Clement JG, *et al*. Pharmacokinetics and biodistribution of amphotericin B in rats following oral administration in a novel lipid-based formulation. J Antimicrob Chemother. 2009;64(1):101–8.
4. Kayser O, Olbrich C, Yardley V, Kiderlen AF, Croft SL. Formulation of amphotericin B as nanosuspension for oral administration. Int J Pharm. 2003;254(1):73–5.
5. Delmas G, Park S, Chen ZW, Tan F, Kashiwazaki R, Zarif L, *et al*. Efficacy of orally delivered cochleates containing amphotericin B in a murine model of aspergillosis. Antimicrob Agents Chemother. 2002;46(8):2704–7.
6. Benson JM, Nahata MC. Pharmacokinetics of amphotericin B in children. Antimicrob Agents Chemother. 1989;33(11):1989–93.
7. Graybill JR. Is there a correlation between serum antifungal drug concentration and clinical outcome? J Infect. 1994;28 Suppl 1:17–24.
8. Bekersky I, Fielding RM, Dressler DE, Lee JW, Buell DN, Walsh TJ. Plasma protein binding of amphotericin B and pharmacokinetics of bound *versus* unbound amphotericin B after administration of intravenous liposomal amphotericin B (AmBisome) and amphotericin B deoxycholate. Antimicrob Agents Chemother. 2002;46(3):834–40.
9. Matsui S, Imai S, Yabuki M, Komuro S. Pharmacokinetics characterization of liposomal amphotericin B: investigation of clearance process and drug interaction potential. Arzneimittelforschung. 2009;59(9):461–70.
10. Hutchaleelaha A, Chow HH, Mayersohn M. Comparative pharmacokinetics and interspecies scaling of amphotericin B in several mammalian species. J Pharm Pharmacol. 1997;49(2):178–83.
11. Atkinson Jr AJ, Bennett JE. Amphotericin B pharmacokinetics in humans. Antimicrob Agents Chemother. 1978;13(2):271–6.
12. Bekersky I, Fielding RM, Dressler DE, Lee JW, Buell DN, Walsh TJ. Pharmacokinetics, excretion, and mass balance of liposomal amphotericin B (AmBisome) and amphotericin B deoxycholate in humans. Antimicrob Agents Chemother. 2002;46(3):828–33.
13. Fielding RM, Smith PC, Wang LH, Porter J, Guo LS. Comparative pharmacokinetics of amphotericin B after administration of a novel colloidal delivery system, ABCD, and a conventional formulation to rats. Antimicrob Agents Chemother. 1991;35(6):1208–13.
14. Gershkovich P, Wasan EK, Sivak O, Li R, Zhu X, Werbovetz KA, *et al*. Visceral leishmaniasis affects liver and spleen concentrations of amphotericin B following administration to mice. J Antimicrob Chemother. 2010;65:535–7.
15. Rowland M, Peck C, Tucker G. Physiologically-based pharmacokinetics in drug development and regulatory science. Annu Rev Pharmacol Toxicol. 2010;51:45–73.
16. Angra PK, Siddig A, Nettey H, Desai N, Oettinger C, D'Souza MJ. Pharmacokinetic and biodistribution studies of amphotericin B microspheres. J Microencapsul. 2009;26(7):627–34.
17. Wang LH, Fielding RM, Smith PC, Guo LS. Comparative tissue distribution and elimination of amphotericin B colloidal dispersion (Amphocil) and Fungizone after repeated dosing in rats. Pharm Res. 1995;12(2):275–83.
18. Chow HH, Cai Y, Mayersohn M. Disposition kinetics of amphotericin B in rats. The influence of dose. Drug Metab Dispos. 1992;20(3):432–5.
19. Chow HH, Wu Y, Mayersohn M. Pharmacokinetics of amphotericin B in rats as a function of dose following constant-rate intravenous infusion. Biopharm Drug Dispos. 1995;16(6):461–73.
20. Robbie G, Chiou WL. Elucidation of human amphotericin B pharmacokinetics: identification of a new potential factor affecting interspecies pharmacokinetic scaling. Pharm Res. 1998;15 (10):1630–6.
21. Brown RP, Delp MD, Lindstedt SL, Rhomberg LR, Beliles RP. Physiological parameter values for physiologically based pharmacokinetic models. Toxicol Ind Health. 1997;13(4):407–84.
22. Davies B, Morris T. Physiological parameters in laboratory animals and humans. Pharm Res. 1993;10(7):1093–5.
23. Gerlowski LE, Jain RK. Physiologically based pharmacokinetic modeling: principles and applications. J Pharm Sci. 1983;72 (10):1103–27.
24. Gibaldi M, Perrier D. Pharmacokinetics. 2nd ed. New York, NY, USA: Marcel Dekker, Inc.; 1982.
25. Rhodin MM, Anderson BJ, Peters AM, Coulthard MG, Wilkins B, Cole M, *et al*. Human renal function maturation: a quantitative description using weight and postmenstrual age. Pediatr Nephrol. 2008;24(1):67–76.

26. Kawai R, Lemaire M, Steimer JL, Bruelisauer A, Niederberger W, Rowland M. Physiologically based pharmacokinetic study on a cyclosporin derivative, SDZ IMM 125. J Pharmacokinet Biopharm. 1994;22(5):327–65.
27. Yamey G, Torreele E. The world's most neglected diseases. BMJ. 2002;325(7357):176–7.
28. Mathers CD, Ezzati M, Lopez AD. Measuring the burden of neglected tropical diseases: the global burden of disease framework. PLoS Negl Trop Dis. 2007;1(2):e114.
29. Christiansen KJ, Bernard EM, Gold JW, Armstrong D. Distribution and activity of amphotericin B in humans. J Infect Dis. 1985;152(5):1037–43.
30. Olivier M, Tanner CE. Susceptibilities of macrophage populations to infection *in vitro* by Leishmania donovani. Infect Immun. 1987;55(2):467–71.
31. Adolph EF. Quantitative relations in the physiological constitutions of mammals. Science. 1949;109(2841):579–85.
32. Wasan EK, Bartlett K, Gershkovich P, Sivak O, Banno B, Wong Z, *et al*. Development and characterization of oral lipid-based Amphotericin B formulations with enhanced drug solubility, stability and antifungal activity in rats infected with *Aspergillus fumigatus* or *Candida albicans*. Int J Pharm. 2009;372(1–2):76–84.
33. Gupta S, Dube A, Vyas SP. Antileishmanial efficacy of amphotericin B bearing emulsomes against experimental visceral leishmaniasis. J Drug Target. 2007;15(6):437–44.
34. Cortadellas O. Initial and long-term efficacy of a lipid emulsion of amphotericin B desoxycholate in the management of canine leishmaniasis. J Vet Intern Med. 2003;17(6):808–12.

View publication stats